Available online at www.sciencedirect.com
ScienceDirect
Applied Catalysis B: Environmental 73 (2007) 247–258
APPLIED CATALYSIS B: ENVIRONMENTAL
www.elsevier.com/locate/apcatb

Effect of Ru on $LaCoO_3$ perovskite-derived catalyst properties tested in oxidative reforming of diesel

R.M. Navarro [a,*], M.C. Alvarez-Galvan [a,*], J.A. Villoria [a], I.D. González-Jiménez [a], F. Rosa [b], J.L.G. Fierro [a]

[a] *Instituto de Catálisis y Petroleoquímica (CSIC), C/Marie Curie no. 2, Cantoblanco 28049 Madrid, Spain*
[b] *Centro de Experimentación de "El Arenosillo" (CEDEA), Instituto Nacional de Técnica Aeroespacial (INTA), Mazagón-Moguer, 21130 Huelva, Spain*

Received 19 October 2006; received in revised form 18 December 2006; accepted 19 December 2006
Available online 30 December 2006

Abstract

The oxidative reforming of diesel over Co/La_2O_3 and $Ru–Co/La_2O_3$ catalysts derived from $LaCoO_3$ perovskite precursors was studied. Physicochemical characterization by XPS, TPR and XRD revealed that the incorporation of Ru to $LaCoO_3$ produces changes in $LaCoO_3$ evidenced by a smaller size of the $LaCoO_3$ particles and cobalt segregation on the $LaCoO_3$ surface. The modifications in the structure of $LaCoO_3$ induced by the addition of Ru directly affect the dispersion and morphology of Co particles developed under the reaction. The active phases derived from pretreatment of perovskites evolve differently with time on stream, being observed that the presence of a greater proportion of perovskite phase in the $Ru/LaCoO_3$ sample produces an increase in catalyst stability. TPD-MS analysis also indicates that bulk oxygen release from the $Ru–Co/La_2O_3$ sample could improve its catalytic behaviour. The characterization of used samples reveals that improvements in the cobalt surface concentration and $Co–La_2O_3$ interactions contribute to the better catalytic stability of the $Ru–Co/La_2O_3$-derived catalyst.

Keywords: $LaCoO_3$ perovskite; Ru; Oxidative reforming; Diesel; Hydrogen production

1. Introduction

The reforming of diesel fuel for the production of hydrogen is difficult because of the refractory nature of the compounds present in diesel fractions [1]. The main problems associated with the reforming of diesel are related to catalyst degradation over time due to the harsh operating conditions (high temperatures and high H_2O/C ratios) necessary to obtain high hydrogen yields. The causes of such degradation include poisoning of the catalysts by sulphur, thermal sintering and extensive coke formation due to the low H:C ratio and the high molecular weight of the molecules present in diesel fuel. Catalyst formulations typically comprise noble (Pt, Rh and Ru) [2,3] or non-noble metals (Ni and Co) deposited or incorporated into carefully engineered supports such as thermally stabilized alumina, doped alumina with promoters to accelerate coke gasification [4], mixed metal oxides [5], as well as metal supported on oxide-ion-conducting substrate like ceria, zirconia or lanthanum gallate doped with non-reducible element such as gadolinium, samarium as those developed at Argonne National Laboratory [3,6].

In the search for catalysts affording catalytic partial oxidation (CPO), steam reforming (SR) and oxidative reforming of hydrocarbons, perovskite oxide precursors are good candidates. This is because perovskite oxide systems with a general formula of ABO_3 (where A and B are usually trivalent rare-earth cations and transition metals, respectively) exhibit very high thermal stability over a broad temperature range as well as high OSC (oxygen storage capacity) and oxygen ion conductivity [7]. Generally speaking, the B-metal site in perovskite oxide forms the primary active site, while the A-metal site has a strong effect on stability and also provides the possibility of improving catalyst performance through synergetic interactions with metals on the B-site. Perovskite oxide precursors not only fulfil the stability requirements for the

* Corresponding authors. Tel.: +34 91 5854773; fax: +34 91 5854760.
E-mail addresses: r.navarro@icp.csic.es (R.M. Navarro), c.alvarez@icp.csic.es (M.C. Alvarez-Galvan).

0926-3373/$ – see front matter © 2007 Elsevier B.V. All rights reserved.
doi:10.1016/j.apcatb.2006.12.013

reforming and oxidation reactions, but may also act as substrates of active particles by reduction of B-site cations, forming a well dispersed and stable metal crystallites over a stable support (oxide of element A) [8–11]. This is very important in view of the reductive conditions during reaction, for which the use of perovskites may allow stabilisation of the small particles of the metal in position B under the reaction conditions [12].

Oxidative reforming, a combination of the SR and PO reactions, was chosen to produce hydrogen since it offers advantages over the individual SR and CPO processes such as the fact that it is less externally energy-intensive, cost effective and it provides a better response to dynamic changes [13]. Moreover, the combination of these reactions can improve the control of the reactor temperature and can reduce the formation of hot spots, preventing catalyst deactivation due to sintering or carbon deposition [14].

The oxidative reforming of hydrocarbons present in diesel fuel can be described by the following reactions:

$$\text{SR}: \quad C_nH_m + nH_2O \rightarrow nCO + (n + m/2)H_2 \tag{1}$$

$$\text{PO}: \quad C_nH_m + n/2O_2 \rightarrow nCO + m/2H_2 \tag{2}$$

with $n = 13$–15 and $m = 26$–30 as mean values.

As indicated in the literature, many transition elements show activity for both the CPO and SR reactions, which means that they could be strong candidates for oxidative reforming [15]. For this work we developed diesel reforming catalysts based on Co on lanthanum oxide derived from $LaCoO_3$ perovskites. Lanthanum was chosen for the A-site, owing to its known promoter effect on both thermal stability and activity [16], whereas cobalt was chosen as the metal at the B-site, taking into account its proven activity for SR reactions [17]. Moreover, $LaCoO_3$ has a high tolerance factor (0.883), which allows the formation of pure perovskite crystallites easily [15]. Both the A- and B-sites in perovskite can be partially exchanged, resulting in mixed valence states and an enhanced mobility of oxygen in the lattice [11]. The exchange at the B-site can also incorporate noble metals, which improve activity, stability and sulphur tolerance [8,18]. Among the transition metals anchored into the perovskite lattice, ruthenium is particularly effective in the catalytic reforming of heavy hydrocarbon fuels [19].

With this background the present work addresses the oxidative reforming of diesel to synthesis gas over Co/La and Ru–Co/La catalysts derived from $LaCoO_3$ perovskites. Several characterization techniques, such as N_2 adsorption–desorption isotherms at 77 K, X-ray diffraction (XRD), X-ray electron spectroscopy (XPS), temperature programmed reduction (TPR), chemical and elemental chemical analysis (ECA), thermogravimetric analysis (TGA) and temperature-programmed desorption-mass spectroscopy (TPD-MS), were used to characterise the fresh, activated and aged catalysts. The surface and structural characteristics of both samples are related to their different catalytic behaviour.

2. Experimental

2.1. Catalyst preparation

$LaCoO_3$ perovskite was prepared by the simultaneous precipitation of cobalt and lanthanum ions using a solution of nitrate salts of cobalt and lanthanum and K_2CO_3 as precipitating agent [20]. The salts $La(NO_3)_3{\cdot}6H_2O$ (99.9%, Johnson Matthey) and $Co(NO_3)_2{\cdot}6H_2O$ (97.7% minimum, Johnson Matthey) were dissolved in distilled water to obtain 1 M solutions. Both solutions were mixed together under vigorous stirring. Then, a stoichiometric quantity plus 10% of an aqueous solution of K_2CO_3 (99.0% minimum, Johnson Matthey) was rapidly added. Under basic (pH > 9) conditions, water was partially evaporated off by heating the solution at around 343 K. Before filtering, the precipitate was washed with ice-cooled distilled water until the pH of the filtrate became neutral. The precursors were then dried at 383 K for 4 h and calcined at 1023 K for 4 h. The heating rate used was 3 K/min from 383 K up to 1023 K. The Ru-added catalyst ($Ru/LaCoO_3$) was prepared by the wet impregnation method, using an appropriate amount of $RuCl_3$ (ruthenium chloride, 48.91% Ru, Premion, Johnson Matthey) to achieve a Ru:La:Co = 0.02:1:1 - molar ratio. Impregnation was carried out in a rotary evaporator at 353 K for 2 h. Then, the samples were dried at 383 K for 4 h and were calcined at 773 K for 3 h. Catalysts based on Ru supported on La_2O_3 (lanthanum oxide, Fluka 99.98%) and Co_3O_4 (prepared by calcination at 823 K for 5 h from $Co(NO_3)_2{\cdot}6H_2O$ Sigma–Aldrich 98%) were prepared by impregnation using above procedure with a Ru:La and Ru:Co molar ratio of 0.02:1 for both catalysts.

2.2. Catalyst characterization

The chemical composition of the calcined catalysts was measured by inductively coupled plasma atomic emission spectroscopy (ICP-AES) on a Perkin-Elmer optima 3300 DV device. Samples were first dissolved in a mixture of acidic solutions of HF, HCl, HNO_3 and H_3PO_4, micro-waved for 40 min, and diluted to concentrations within the calibration range of the instrument.

The BET surface area of the perovskite precursors prepared were calculated from the nitrogen adsorption–desorption isotherms obtained at the temperature of liquid nitrogen (77 K), taking a value of 0.162 nm^2 for the cross-section of N_2 molecule adsorbed at this temperature. These measurements were performed with a Micromeritics ASAP 2100 apparatus on samples previously degassed at 423 K for 12 h.

XRD patterns were recorded using a Seifert 3000P vertical diffractometer and nickel-filtered Cu Kα radiation ($\lambda = 0.1538$ nm) under constant instrumental parameters. For each sample, Bragg angles between 5° and 80° were scanned; a rate of 5 s per step (step size: 0.04° 2θ) was used during a continuous scan in the above-mentioned range. The mean $LaCoO_3$, La_2O_3 and Co^0 particle size was then estimated from X-ray line width broadening using the Scherrer equation. Width (t) was taken as the full width at half maximum intensity of the

most intense and least overlapped peak ($2\theta = 47.5^\circ$, 29.9° and 44.2°, respectively).

XPS measurements were recorded using a Escalab 200R spectrometer equipped with a hemispherical electron analyser and an Al Kα ($h\nu = 1486.6$ eV, 1 eV = 1.6302×10^{-19} J) 120 W X-ray source. The area of the peaks was estimated by calculating the integral of each peak after smoothing and subtraction of an S-shaped background and fitting of the experimental curve to a mixture of Lorentzian and Gaussian lines of variable proportions. All binding energies (BE) were referenced to the C 1s signal at 284.6 eV from carbon contamination of the samples to correct the charging effects. Quantification of the atomic fractions on the sample surface was obtained by integration of the peaks with appropriate corrections for sensitivity factors [21].

Hydrogen temperature-programmed reductions (H_2-TPR) of the catalysts were conducted using a Micromeritics 2900 instrument in a U-shaped quartz reactor. Prior to the reduction experiments, the sample (30 mg) was flushed with a helium stream at 383 K for 15 min and then cooled down to room temperature. TPR profiles were obtained by heating the sample under a 10% H_2/Ar flow (50 mL/min) from 303 to 1273 K at a linearly programmed rate of 10 K/min.

The amount of adsorbed compounds as well as the decomposition of perovskite samples during pretreatment were determined by thermogravimetric analysis (TGA/SDTA 851e Mettler Toledo), measuring the weight change of the calcined samples during heating at high temperature. Analyses were carried out by raising the sample temperature from 298 to 1123 K at a rate of 5 K/min in a N_2 flow.

Determination of the thermal stability of oxygen and also of the adsorbed molecules was accomplished by temperature-programmed decomposition and desorption in flowing argon. TPD-MS of the above-mentioned compounds present in the calcined samples was carried out by flowing 20 mL N/min of Ar through the system while the sample was heated at 10 K/min. About 80 mg of the sample was loaded into a U-shaped quartz reactor connected on-line with a quadrupole mass spectrometer (Balzers QMS 200), allowing analysis of the gas phase at the reactor exit. A temperature ramp was started from 303 to 1123 K and was maintained at this temperature for 15 min, while the fragments with $m/z = 18$, 32 and 44, corresponding to water, oxygen and CO_2, respectively were monitored continuously.

ECA was performed to determine the carbon content in the used catalysts. This was accomplished using a Leco CHNS-932 device with an AD-4 Perkin-Elmer autobalance (resolution 0.1 μg).

2.3. Activity tests

Catalytic tests were carried out in a fixed-bed continuous-flow stainless steel reactor. The catalytic bed – 100 mg of catalyst diluted with SiC ($d_p = 0.5$ mm; SiC/catalyst = 5 volume) to avoid preferential gas flow parts and hot spots – was placed in a tubular reactor (8-mm i.d.) with a coaxially centred thermocouple in contact with the catalytic bed. Prior to the reaction, perovskite precursors were flushed in helium at 1123 K before admission of the feed mixture. The flow rates of the diesel and water feeds were controlled by liquid pumps and the feeds were preheated to 623 K in an evaporator before being passed through the catalyst bed in the reactor. Diesel has been provided by CEPSA (R&D Center) and its sulphur amount is 12 ppm. Nitrogen gas (2 mL/min) was also fed into the evaporator to facilitate the evaporation and passage of both the hydrocarbon and water. For the oxidative reforming of diesel, the reactants were introduced into the reactor at a molar ratio of $H_2O/O_2/C = 3/0.5/1$. The total gas flow rate was kept at 75 mL/min (GHSV = 20,000 h^{-1}). Activity was measured at atmospheric pressure and 1023 K (25 h) or 1123 K (60–80 h). The products were analysed periodically with an on-line gas chromatograph (HP 5890 Series II) equipped with a TC detector which was programmed to operate under high-sensitivity conditions. A 4A-molecular sieve column was used for H_2, O_2, N_2, CO and CH_4 separation and a Porapack N (80/100) for CO_2, C_2H_4, C_2H_6 and H_2O. The diesel conversion and hydrogen yield were defined as follows:

$$\text{conversion}\,(\%) = \frac{\text{mole amount of C components in reformate}}{\text{total mole amount of C in feed}C_nH_m} \times 100 \quad (3)$$

$$\text{yield}\,(\%)\left(\frac{\text{mol}\,H_2}{\text{mol}\,C}\right) = \frac{\text{mole amount of}H_2\text{ in reformate}}{\text{total mole amount of C in feed}C_nH_m} \times 100 \quad (4)$$

$$\text{yield}\,(\%)\left(\frac{\text{mol}\,H_2 + CO}{\text{mol}\,C}\right) = \frac{\text{mole amount of}H_2 + CO\text{ in reformate}}{\text{total mole amount of C in feed}C_nH_m} \times 100 \quad (5)$$

3. Results

3.1. Characterization of calcined and pretreated perovskites

3.1.1. Chemical composition (ICP-AES)

The chemical composition (wt%) of the calcined samples was determined by ICP-AES and the results are summarized in Table 1. The results indicate that the Co/La ratio approaches the stoichiometric value. In addition, the concentration of ruthenium for Ru-containing sample was close to nominal value, indicating the effectiveness of the catalyst preparation procedure.

Table 1
Chemical composition (wt%) of calcined $LaCoO_3$ and $Ru/LaCoO_3$ samples

Sample	% Co	% La	% Ru
$LaCoO_3$	23.1	54.5	0
$Ru/LaCoO_3$	23.7	55.9	0.7

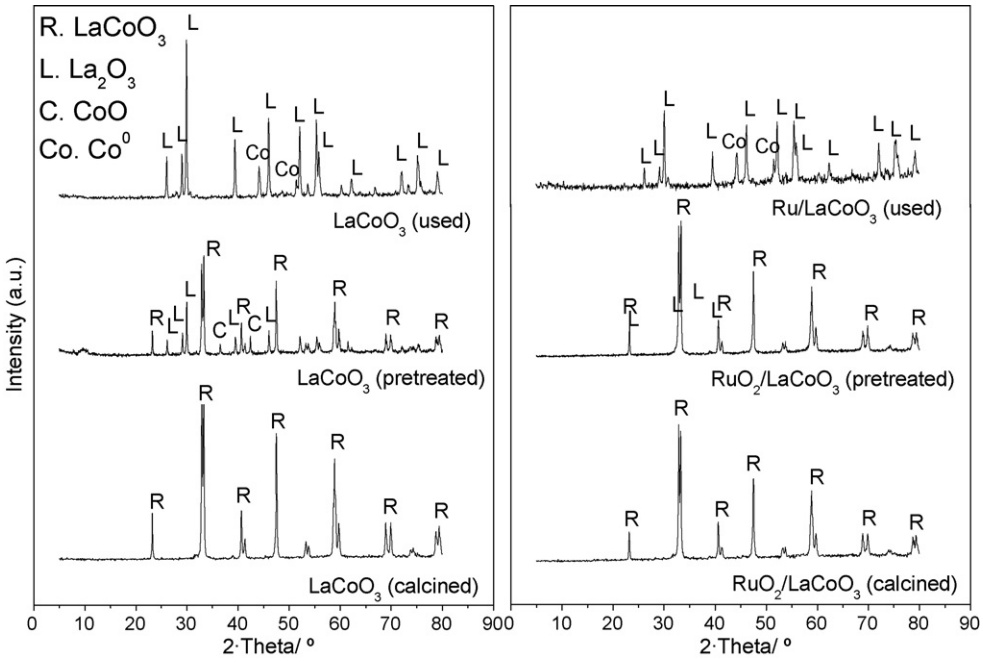

Fig. 1. XRD patterns of $LaCoO_3$ and $Ru/LaCoO_3$ (calcined, pretreated under inert gas at 1123 K and used).

3.1.2. BET surface area and XRD

Textural data obtained from N_2 adsorption–desorption isotherms disclosed a BET surface area for calcined $LaCoO_3$ and $Ru/LaCoO_3$ samples of 3.3 and 7.2 m^2/g, respectively. Taking into account that the BET surface area of the perovskite powders is equal to the geometrical area, since they do not possess internal microporosity, the changes observed in the surface area with the incorporation of Ru suggest changes in the particle size of $LaCoO_3$ during Ru deposition. Fig. 1 shows the XRD patterns of the calcined and pretreated (after pretreatment under He at 1123 K) $LaCoO_3$ and $Ru/LaCoO_3$ samples. The XRD pattern of the calcined $LaCoO_3$ exhibits strong reflections at 32.9° (1 1 0) and 33.3° (1 0 4), corresponding to stoichiometric perovskite with a rhombohedral distortion of the ideal cubic structure of perovskite (JCPDF 48-123). No segregated phases corresponding to La or Co oxides were detected. As may be observed in Fig. 1, treatment in He at 1123 K resulted not only in a decrease in the peak heights assigned to the $LaCoO_3$ perovskite phase but also in the appearance of diffraction lines corresponding to La_2O_3 (JCPDF 74-2430) and CoO (JCPDF 43-1004). This finding is conclusive of the partial decomposition of $LaCoO_3$ perovskite during the pretreatment in inert atmosphere.

The XRD pattern of the calcined $Ru/LaCoO_3$ sample only displayed the diffraction lines previously observed in calcined $LaCoO_3$, corresponding to a rhombohedrally distorted perovskite structure. The peaks related to RuO_2 are not visible, possibly due to the low concentration of ruthenium added to the $LaCoO_3$. The presence of segregated phases associated with La or Co was not observed. Nevertheless, the presence of La/Co phases at a very low concentration and/or an amorphous state cannot be discarded because of the detection limit (ca. 4 nm) of the XRD technique. As seen in Fig. 1, the pretreatment in He of the $Ru/LaCoO_3$ did not elicit any loss of crystallinity, as previously observed for the bare $LaCoO_3$. Quantitative estimation of the crystallite sizes of the $LaCoO_3$ phase by applying the Scherrer equation (Table 2) was also performed by taking the broadening of the (0 2 4) reflection of the $LaCoO_3$ phase (at 2θ angle of 47.5°). It may be noted that the mean crystallite size of calcined $Ru/LaCoO_3$ was slightly lower than the bare $LaCoO_3$ counterpart. After pretreatment under He, an increase in the $LaCoO_3$ mean crystallite size of the bare $LaCoO_3$ was observed, while for the $Ru/LaCoO_3$ counterpart no apparent change in the size of the $LaCoO_3$ crystallites was detected.

3.1.3. XPS

XPS was used to determine the chemical state of the elements and their surface proportions in the calcined and thermally treated $LaCoO_3$ and $Ru/LaCoO_3$ samples. Fig. 2 compares the Co 2p core-level spectra for the $LaCoO_3$ and $Ru/LaCoO_3$ samples, both calcined and treated thermally under He at 1123 K. The $LaCoO_3$ calcined sample exhibited the Co $2p_{3/2}$ peak at a binding energy close to 779.0 eV. This value is lower than that typically reported for cobalt oxides [22]. The BE value for Co $2p_{3/2}$, together with the weakness of the shake-up peaks, indicates that on the calcined $LaCoO_3$ sample surface cobalt atoms mainly form an $LaCoO_3$ phase. Table 3 summarizes the

Table 2
Mean crystallite size according to the Scherrer equation

	$LaCoO_3$ mean diameter (nm)	
	$LaCoO_3$	$Ru/LaCoO_3$
Calcined	44	42
Pretreated	48	43

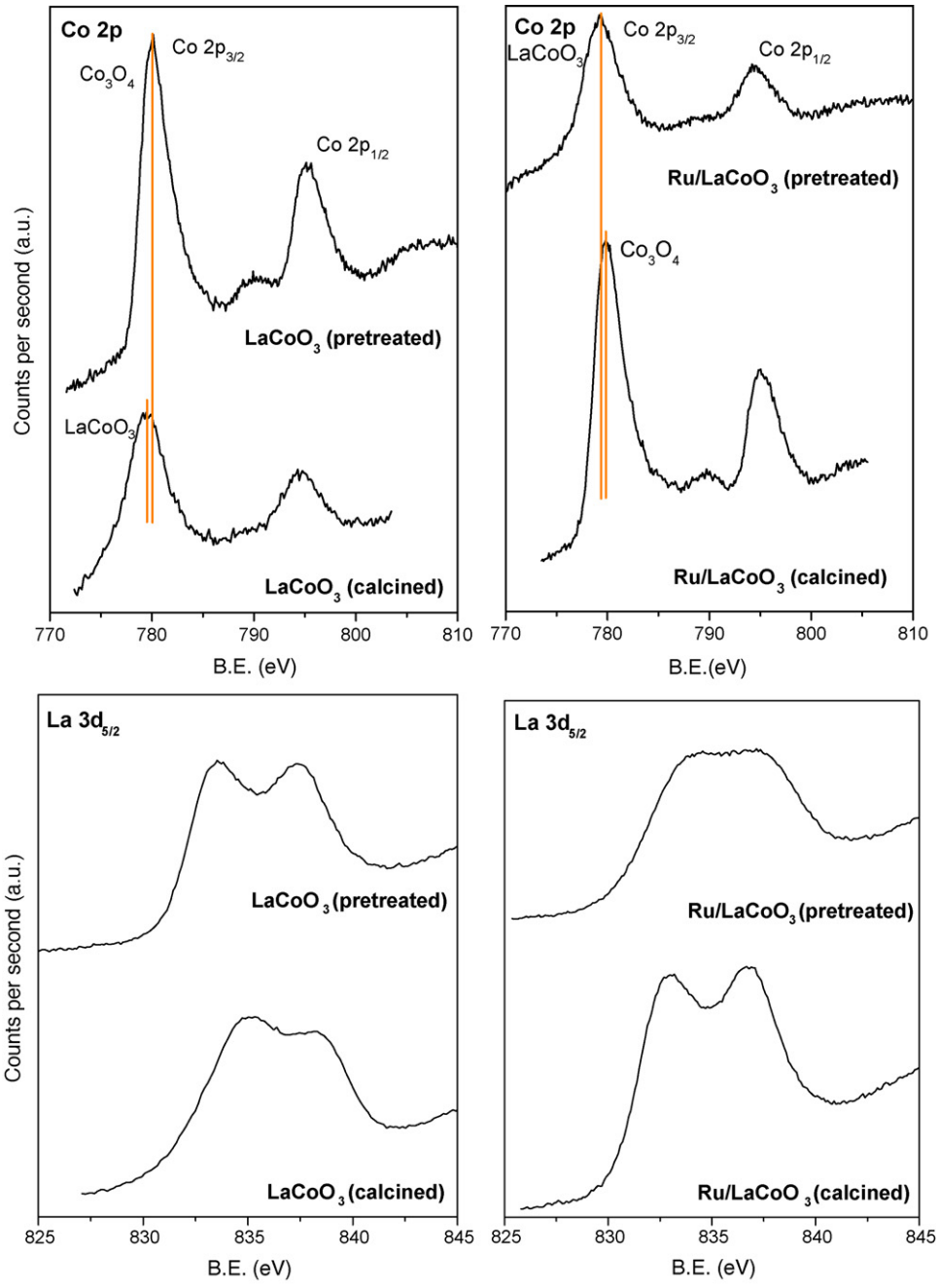

Fig. 2. Co 2p and La $3d_{5/2}$ XPS spectra of calcined and pretreated $LaCoO_3$ and $Ru/LaCoO_3$ samples.

atomic surface Co/La ratios. The measured surface Co/La ratio for calcined $LaCoO_3$ is lower than the nominal ratio. This lower Co/La ratio may be explained in terms of a segregation of La to the surface. This effect is also found in other $LaMO_3$ perovskites and is due to the basicity of La^{3+} cations and their tendency to react with atmospheric CO_2 and H_2O [23]. As shown in Fig. 2, after pretreatment under He the Co $2p_{3/2}$ level of $LaCoO_3$ displayed a single peak at 780.1 eV and a shake-up component at ca. 790.0 eV, indicative of the presence of surface Co_3O_4 species. This points to surface changes in the perovskite structure of $LaCoO_3$ after pretreatment. The changes in $LaCoO_3$ also modified Co/La surface concentrations, leading to cobalt surface enrichment, as indicated by the higher Co/La shown in Table 3.

Table 3
Surface Co/La (XPS) for the calcined and pretreated $LaCoO_3$ and $Ru/LaCoO_3$ samples

	Co/La	
	$LaCoO_3$	$Ru/LaCoO_3$
Calcined	0.76	1.12
Pretreated	1.63	0.78

This surface change from the $LaCoO_3$ phase in the calcined $LaCoO_3$ sample to a partial decomposed perovskite in its corresponding La and Co oxides when it is pretreated in inert

gas is also supported upon scrutiny of the La $3d_{5/2}$ core-level. As reported in the literature [24], in the $LaCoO_3$ calcined sample the La 3d doublets are ill-defined; however when the sample was pretreated in helium the doublets were better resolved and more similar to the spectrum of La_2O_3. Thus, as shown in Fig. 2, the La $3d_{5/2}$ spectrum in the $LaCoO_3$ calcined sample mainly displays a phase constituted by La in the form of $LaCoO_3$, while when it was treated in He up to 1123 K, the XPS spectrum corresponds to La in the form of La_2O_3. For calcined $Ru/LaCoO_3$ (Fig. 2), the binding energy of the Co $2p_{3/2}$ level and the characteristic shake-up satellite line at ca. 790.0 eV suggest the presence of Co_3O_4 at the surface. The measured Co/La ratio for this calcined sample (Table 3) was higher than the nominal ratio, indicating segregation of the cobalt phase to the surface, probably induced by the ruthenium deposition step. The chemical changes brought about by treatment of the $Ru/LaCoO_3$ sample in inert gas at 1123 K were also revealed by XPS. As shown in Fig. 2, after pretreatment the Co $2p_{3/2}$ shifted to a lower binding energy and the shake-up peak decreased. Both these observations suggest the presence of surface Co-forming $LaCoO_3$ phases. The surface changes after treatment in inert gas at high temperature also affected surface composition. Table 3 shows a decrease in the Co/La ratio after pretreatment, a value close to that corresponding to bare calcined $LaCoO_3$ being reached. This change in the surface composition undergone upon sample treatment in helium is also observed in the La 3d peaks. As seen in Fig. 2, the surface of the Ru-containing sample should mainly be constituted by the La_2O_3 phase, since it displays a well resolved La $3d_{5/2}$ profile. When this sample was activated in inert gas, an ill-resolved La 3d doublet was obtained, indicative of the presence of La^{3+} in the $LaCoO_3$ structure.

Regarding the chemical nature of ruthenium, it should be noted that the most intense Ru $3d_{5/2}$ component was overshadowed by a strong C 1s line appearing in the same energy region. Thus, another less intense Ru $3p_{3/2}$ line was recorded and used for this purpose. Fig. 3 shows the Ru $3p_{3/2}$ spectra for both the calcined and pretreated $Ru/LaCoO_3$ samples. A shift to 462.8 eV in the pretreated sample with respect to that at 464.0 eV in the calcined sample may be observed. This finding could be due to a reduction of RuO_2 to Ru^0 upon treatment with helium [25].

3.1.4. TPR

The TPR profiles of the calcined $LaCoO_3$ and $Ru/LaCoO_3$ samples are shown in Fig. 4. The reduction profile of $LaCoO_3$ clearly indicates that reduction proceeds according to two consecutive steps. The reduction mechanism of $LaCoO_3$, however, is controversial. Studies reported in literature [26,27] have proposed that the reduction of Co^{3+} in $LaCoO_3$ occurs through the following two steps:

$$2LaCoO_3 + H_2 \rightarrow 2LaCoO_{2.5} + H_2O \quad (6)$$

$$2LaCoO_{2.5} + 2H_2 \rightarrow La_2O_3 + 2Co^0 + 2H_2O \quad (7)$$

Thus, the TPR profile of $LaCoO_3$ shows two separate peaks at around 693 and 823 K, which were assigned to the consecutive reduction of Co^{3+} to Co^{2+} in the form of $LaCoO_{2.5}$ and to Co^0 finely dispersed on La_2O_3, respectively. The position of the afore-mentioned peaks depends on the kinetics of the reduction, which is mainly influenced by crystallite size and oxygen defects in the perovskite lattice [28,29]. The shoulder at 623 K (Fig. 4) can be assigned to the reduction of a low

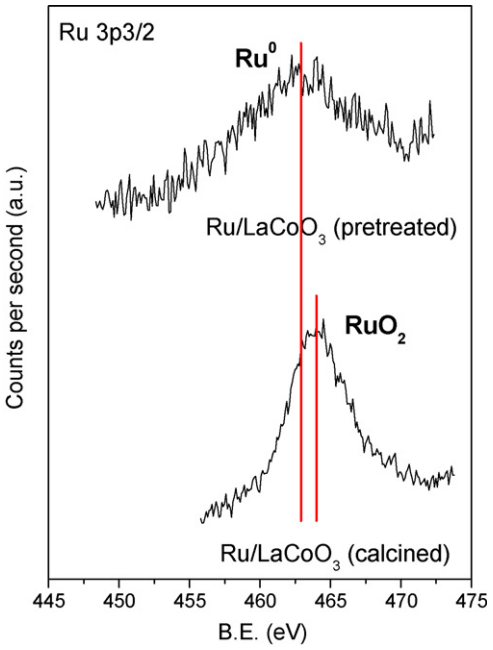

Fig. 3. Ru $3p_{3/2}$ XPS spectra of calcined and pretreated $Ru/LaCoO_3$ sample.

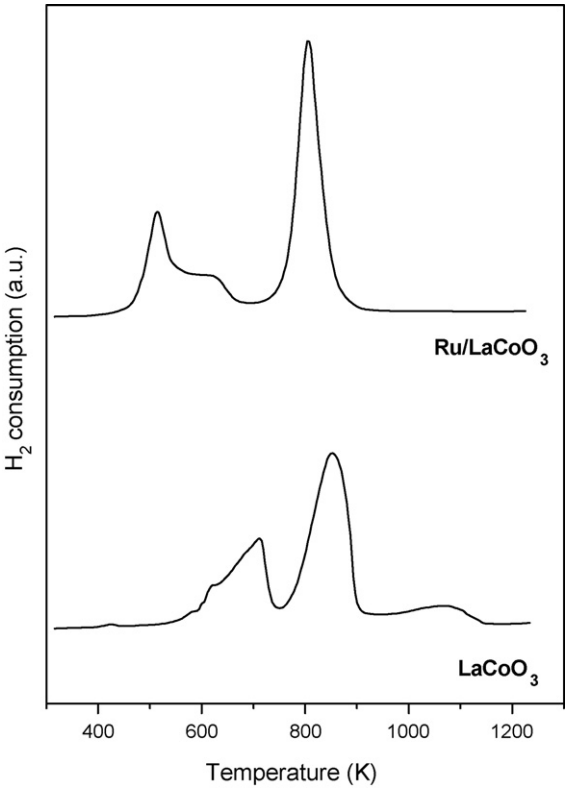

Fig. 4. TPR profiles of $LaCoO_3$ and $Ru/LaCoO_3$ precursors.

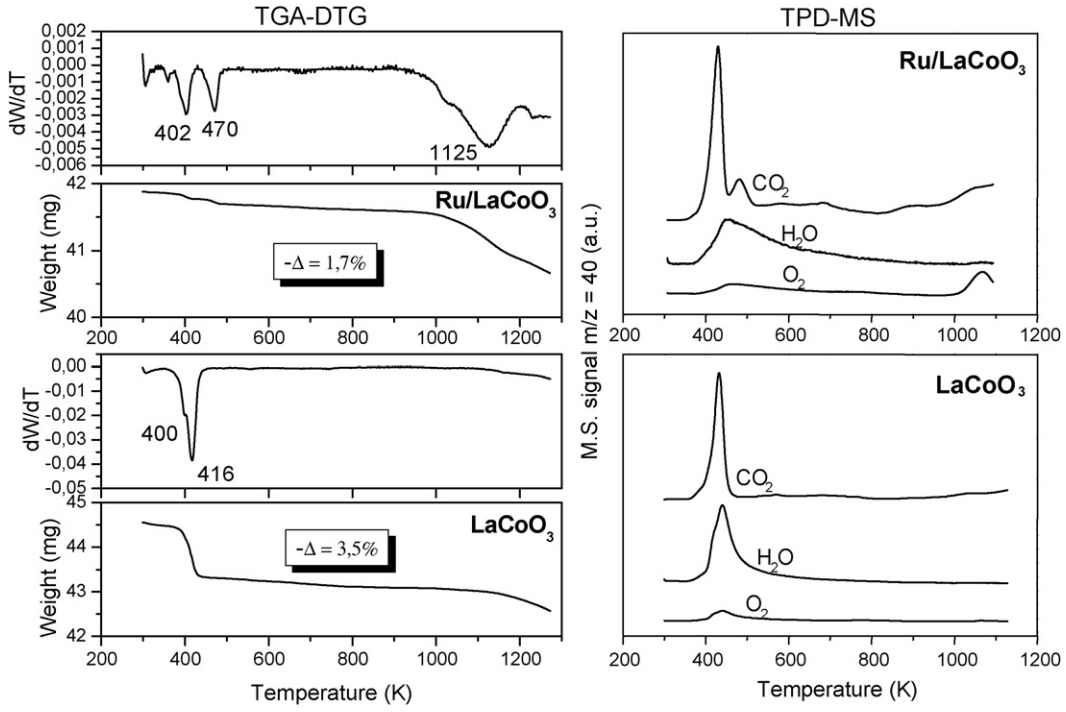

Fig. 5. TGA–DTG analysis curves and TPD-MS spectra for $LaCoO_3$ and $Ru/LaCoO_3$ calcined samples.

proportion of cobalt oxide phases as small crystallites, not detected by XRD.

For the Ru-containing $LaCoO_3$ sample, three H_2-consumption peaks (493, 623 and 803 K) are observed. The peaks at 623 and 803 K are associated with a reduction of the $LaCoO_3$ phase while the additional low temperature peak could be due to the reduction of cobalt oxide phases. Upon scrutiny of the reduction temperatures, a marked effect of Ru on the reducibility of both cobalt oxides and the $LaCoO_3$ phase is seen. According to the literature, Ru would facilitate the reduction of cobalt oxides [30] through the formation of Co–Ru oxides [31] that are reduced at lower temperatures, or through a spill-over process with hydrogen species activated and dissociated on ruthenium metallic phases [32]. The peaks corresponding to the two-step reduction of the $LaCoO_3$ phase also shift to lower temperatures with the addition of Ru. This better reducibility of $LaCoO_3$ may be associated with the above spill-over process assisted by ruthenium, or more probably to changes in the perovskite crystal size/structure during Ru deposition, leading to structures with lower diffusional resistance to hydrogen reduction.

3.1.5. TGA

The decomposition behaviour of the calcined samples was studied by thermogravimetric analysis (TGA). Both the TGA curves and the respective derivative profiles of the $LaCoO_3$ and $Ru/LaCoO_3$ samples are shown in Fig. 5. In the case of the $LaCoO_3$ sample, the derivative curve indicates that the main weight loss occurred at 416 K (with a lesser contribution at 400 K), whereas the $Ru/LaCoO_3$ sample shows weight losses at 402, 470 and 1125 K. Weight loss after treatment in an inert atmosphere up to reaction temperature (1123 K) for $LaCoO_3$ is 3.5%, which is substantially higher than the 1.7% found for the $Ru/LaCoO_3$ sample. Since both the CO_2 and H_2O products are desorbed during treatment, TPD-MS analysis of the gaseous effluents from the TPD cell was carried out.

3.1.6. TPD-MS analysis

TPD-MS analysis for both the $LaCoO_3$ and $Ru/LaCoO_3$ samples was performed under an inert atmosphere to evaluate the desorption of different molecules. The two $LaCoO_3$ and $Ru/LaCoO_3$ calcined samples desorbed H_2O, O_2 and CO_2 with increasing temperature (Fig. 5). A water desorption peak was observed between 400 and 600 K for the $LaCoO_3$ sample and between 400 and 800 K for the $Ru/LaCoO_3$ sample. Simultaneously, CO_2 is desorbed at between 350 and 480 K for $LaCoO_3$ and at between 350 and 530 K for $Ru/LaCoO_3$. As reported in the literature [33], upon exposure to atmospheric H_2O and CO_2 at room temperature, lanthana thoroughly transforms into a partly carbonated hydroxide, actually consisting of a nucleus of crystalline $La(OH)_3$ surrounded by a few layers of a heavily disordered hydroxycarbonated phase. The following thermal decomposition scheme may be proposed [33]:

$$\begin{array}{l} La(OH)_3 \\ La(OH)_x(CO_3)_y \end{array} \xrightarrow{-H_2O} \begin{array}{l} LaO(OH) \\ La_2(OH)_2CO_3 \end{array} \xrightarrow{-H_2O} \begin{array}{l} La_2O_3 \\ La_2O_2CO_3 \end{array} \xrightarrow{-CO_2} La_2O_3 \quad (8)$$

The profiles recorded for the desorption of H_2O and CO_2 show maxima at temperatures lower than bulk lanthana and that are close to those reported in previous studies [33] for supported lanthana. The presence of lanthana at the surface of $LaCoO_3$ sample is in accordance with the shape of its XPS La $3d_{5/2}$

spectrum, since, as previously commented, it does not correspond to a pure $LaCoO_3$ phase. The broader profiles of the H_2O and CO_2 desorptions for the Ru-containing sample could be explained on the basis of the higher proportion of surface lanthana in this sample, as previously commented in the results of the XPS analyses.

The oxygen TPD signal for perovskite-like oxides is usually attributed to the release of oxygen species situated in structural defects, mainly oxygen from the bulk [34]. However, since a relatively large number of structural defects are present in these catalysts, part of the desorbing oxygen could also be due to surface species. The energetically most labile oxygen desorbed at lower temperatures in the 400–500 K region can essentially be related to simple surface chemisorption, whereas the larger quantity desorbed at higher temperatures (above 1020 K) and observed in TPD profile of $Ru/LaCoO_3$ would be related to mobile bulk oxygen associated with the defective perovskite structure and linked to redox transitions of the valence state of the B ion [35,36]. The desorption temperature for this bulk oxygen is similar to that obtained in the DTG profile.

3.2. Activity and stability tests

The activity of the $LaCoO_3$ and $Ru–LaCoO_3$ samples pretreated in He at 1123 K was evaluated in the oxidative reforming of diesel, performed – as indicated in the experimental section – at atmospheric pressure, 20,000 h^{-1} and at 1023 (for 25 h) and 1123 K (for 60 and 80 h). Fig. 6 shows the evolution of the hydrogen yield as the primary hydrogen produced during oxidative reforming (graphs at the top) and also the potential hydrogen (primary and that produced during the WGS reaction) (graphs at the bottom) by carbon atom in the feed as a function of the reaction time. For both catalysts, diesel conversion reached 100% and was maintained with the reaction time at 1123 K. Although the total diesel conversion persisted with the reaction time on the $LaCoO_3$-derived catalyst, the product distribution changed with time-on-stream, as shown in Fig. 6. The reaction over $LaCoO_3$ began with high selectivity to H_2 and CO but the product distribution changed in the first hours on-stream. As observed in Fig. 6A, hydrogen and CO concentrations decrease to about 40% along the 80 h of reaction. In contrast with the bare perovskite catalyst, the activity of the $Ru/LaCoO_3$-derived catalyst remained high and stable throughout the 80 h of reaction. An excellent hydrogen yield (90%, with respect to the maximum theoretical value, including the fraction produced by WGS) was obtained for this catalyst formulation during the 80 h of the oxidative reforming of commercial diesel. The activity and stability results achieved for this catalyst were similar to the best results obtained for diesel reforming published in the open literature [19]. This better catalytic behaviour of $Ru/LaCoO_3$-derived catalyst if compared to $LaCoO_3$ counterpart has been confirmed with another activity tests during 60 h of reaction at 1123 K (Fig. 6B) and during 25 h of reaction at 1023 K (Fig. 6C), obtaining a mean conversion value of 80% for this lower reaction temperature.

The effect of ruthenium, cobalt and lanthanum oxide over the capacity to extract hydrogen from diesel has been studied by testing the activity of Ru/Co_3O_4 and Ru/La_2O_3 catalysts. The obtained results are shown in Fig. 6A and indicate that, although a high yield toward hydrogen is obtained for these Ru-based catalysts at the beginning of reaction, a deactivation process occurred along the 80 h of reaction, being greater for Ru/Co_3O_4.

Fig. 7 shows the gaseous product compositions as a function of reaction time for both catalysts during the 80 h of the

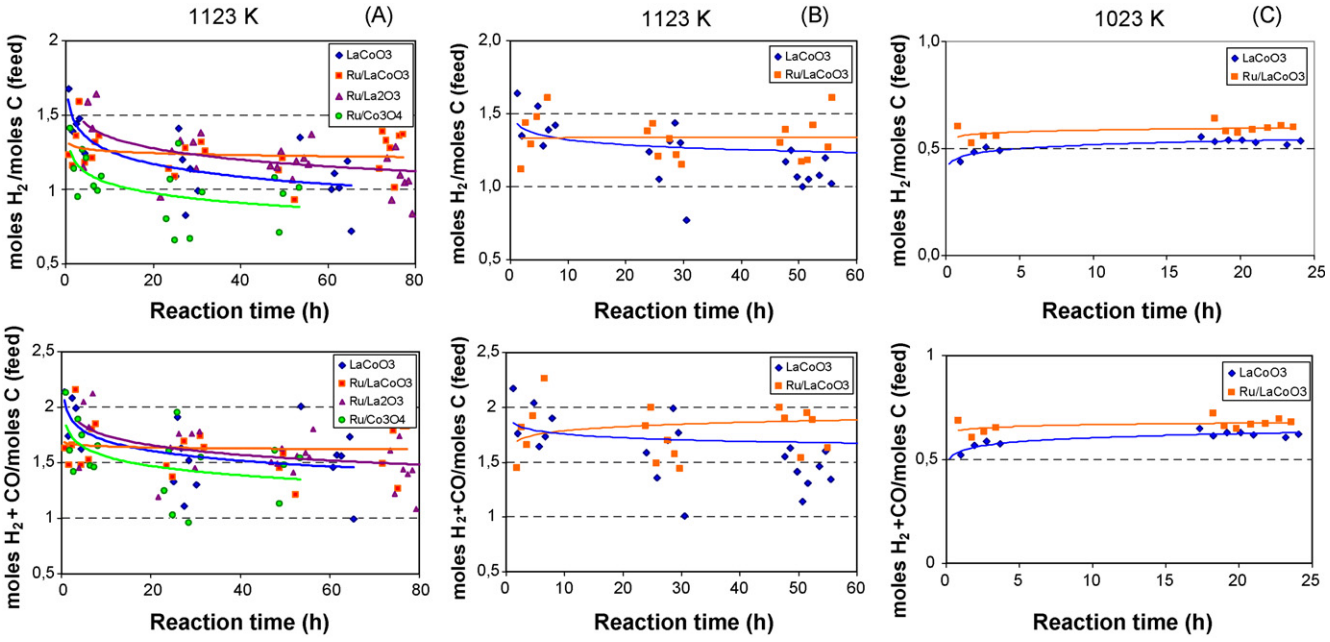

Fig. 6. Hydrogen yield during oxidative reforming of diesel over $LaCoO_3$- and $Ru/LaCoO_3$-derived catalysts as a function of reaction time (A: 1123 K, 20,000 h^{-1}, 80 h; B: 1123 K, 20,000 h^{-1}, 60 h; C: 1023 K, 20,000 h^{-1}, 25 h).

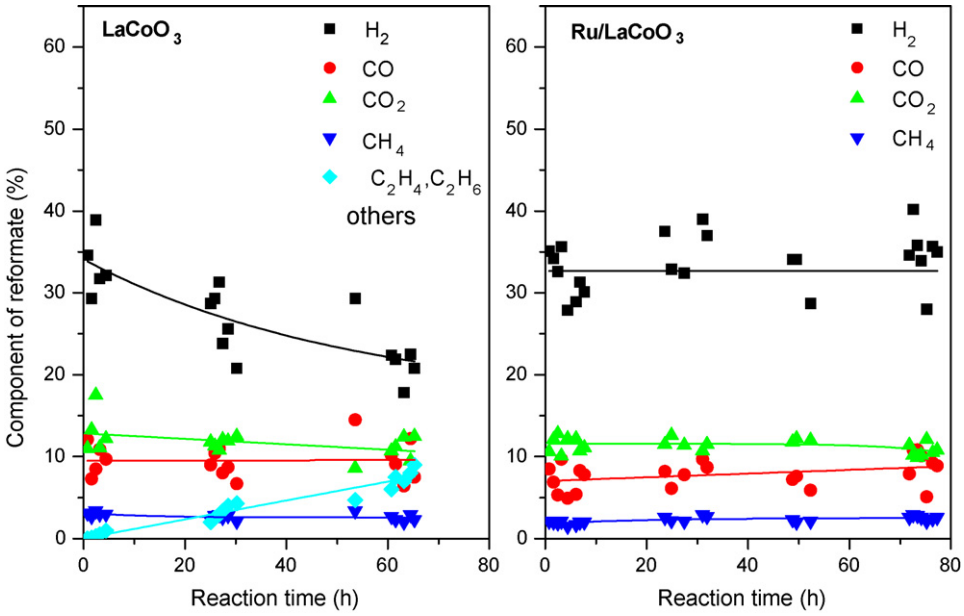

Fig. 7. Product distribution (mol%) in reformate for $LaCoO_3$- and $Ru/LaCoO_3$-derived catalysts as a function of reaction time (1123 K, 20,000 h^{-1}, 80 h).

oxidative reforming of commercial diesel at 1123 K. Comparison of the molar fractions towards the diverse reaction products also revealed differences for the Ru-containing and Ru-free $LaCoO_3$-derived catalysts. A lower degree of hydrogen extraction as well as a higher proportion of hydrogen-containing molecules such as methane, ethane and ethylene and other olefin products, were observed for bare $LaCoO_3$-based catalysts with respect to those obtained on the Ru-containing counterpart.

3.3. Characterization of used catalysts

3.3.1. XRD

The diffraction patterns of the used catalysts are shown in Fig. 1. None of the used samples showed diffraction peaks corresponding to crystalline forms of graphitic carbon at $2\theta = 26.2^\circ$ (JCPDF 75-1621). Both used samples exhibited reflections corresponding to La_2O_3 (JCPDF 74-2430) and metallic Co (JCPDF 15-806). As observed in Fig. 1, the diffraction lines corresponding to the metallic Co and La_2O_3 phases reveal a higher degree of definition and intensity for the used $LaCoO_3$-derived catalyst than for the Ru-containing counterpart. Quantitative estimation of the crystalline domains of Co^0 and La_2O_3 in the used samples by applying the Scherrer equation (Table 4) indicated the larger Co^0 and La_2O_3 crystal size after reaction for the $LaCoO_3$-derived catalyst than for that of the $Ru/LaCoO_3$ counterpart.

3.3.2. XPS

XPS analyses of the $LaCoO_3$- and $Ru/LaCoO_3$-derived catalysts used in the oxidative reforming of diesel were also performed to determine the evolution of active phases after the reaction. The binding energy for the Co $2p_{3/2}$ core level of the used catalysts appeared at 778.0 eV. This binding energy corresponds to metallic Co surface species. The calculated XPS Co/La ratio for the used samples (Table 4) revealed differences in Co surface exposure after the reaction. A higher degree of Co exposure was observed for the used Ru-containing catalyst with respect to that calculated for the bare perovskite-derived catalyst.

The O 1s XPS signal of the used $LaCoO_3$- and $Ru/LaCoO_3$-derived catalysts shows two main photolines at 529.0 eV and 530.8 eV. According to the literature [37], the low binding energy peak should be assigned to lattice oxygen and the high binding energy to adsorbed oxygen species (such as carbonates associated with La_2O_3). The relative concentration of both oxygen species was calculated and is summarized in Table 4. As seen in this table, the calculated adsorbed/lattice oxygen ratio was higher for the $Ru/LaCoO_3$-derived catalysts, indicating a greater proportion of surface carbonates in the $La_2O_2CO_3$ form at the surface of this sample with respect to the used bare perovskite counterpart [38].

3.3.3. ECA

Elemental chemical analyses of the used $LaCoO_3$- and $Ru/LaCoO_3$-derived catalysts were carried out to calculate the

Table 4
Different properties of the used catalysts

Used catalysts	Surface Co/La (XPS)	O_{ad}/O_{lat} (XPS)	$d_{La_2O_3}$ (XRD)	d^0_{Co} (XRD)	% C (ECA)
$LaCoO_3$	0.68	1.12	51	43	0.84
$Ru/LaCoO_3$	1.18	1.77	37	36	0.56

amount of carbonaceous residues retained in the catalysts after the reaction by measuring the quantity of CO_2 produced during its temperature-programmed oxidation under an oxygen gas flow. The coke content in the used catalysts shown in Table 4 was calculated from the amount of CO_2 produced within the temperature 573 and 1100 K range. For both samples, the coke content after the reaction was low. Nevertheless, differences in surface coke formation were observed, depending on the nature of catalyst. In this sense, a lower carbon deposition was observed (Table 4) for the Ru-added catalyst (0.6 wt%) with respect to the bare-perovskite counterpart (0.8 wt%).

4. Discussion

Physicochemical characterization of the calcined perovskite precursors revealed that the deposition of Ru on $LaCoO_3$ modifies its properties at different levels. Changes in particle size after Ru deposition were observed in the BET and XRD results. The higher BET area together with the lower intensity of the XRD peaks observed for $Ru/LaCoO_3$ (Fig. 1) are indicative of a decrease in a particle size of the $LaCoO_3$ crystallites after Ru deposition. The shift in the reduction temperatures of $LaCoO_3$ observed in the TPR experiments on calcined $Ru/LaCoO_3$ corroborates the reorganization of $LaCoO_3$ during Ru deposition, leading to a lower particle size of the $LaCoO_3$ crystallites. Partial dissolution of $LaCoO_3$ during Ru deposition may lie at the origin of the observed changes in particle size as well as the partial segregation of the cobalt phase towards the surface detected by XPS (Table 3). The modifications in $LaCoO_3$ due to the addition of Ru directly affect the structure and morphology of the Co particles after the pretreatment in an inert atmosphere prior to the reaction. For bare $LaCoO_3$, this treatment led to its partial decomposition into lanthanum and cobalt oxide, as indicated by the XRD (Fig. 1) and XPS (Fig. 2) data. By contrast, this partial decomposition seen after pretreatment was not observed in the case of $Ru/LaCoO_3$, this sample maintaining the perovskite structure of $LaCoO_3$. The better stability of $Ru/LaCoO_3$ is probably related not only to the morphological properties of the $LaCoO_3$ crystallites but also to the presence of cobalt and lanthanum oxides at the surface of the $LaCoO_3$ after Ru deposition, which may hinder oxygen diffusion from the $LaCoO_3$ lattice, thus modifying the perovskite decomposition process under pretreatment.

Activity measurements coupled with the physicochemical characterization of the used catalysts show that the dispersed transition metal on the surface of the lanthanum oxide plays an essential role in the catalytic behaviour of the perovskite-derived catalysts. Despite the intrinsic reforming capacity of ruthenium, comparison of the initial activity ($LaCoO_3 > Ru/LaCoO_3$, Fig. 6) and the surface cobalt concentration ($LaCoO_3 > Ru/LaCoO_3$, Table 2) indicates that the higher initial activity observed for the bare $LaCoO_3$-derived catalysts may be related to the higher cobalt concentration achieved after thermal decomposition in this sample with respect to that corresponding to $Ru/LaCoO_3$. The active phases at the beginning of the reaction evolve differently with time on-stream. It was found that the presence of an extended perovskite phase, whose proportion increased in $Ru/LaCoO_3$, produced an increase in catalyst stability (Fig. 6). Changes in the cobalt surface concentration must be considered in order to explain the evolution of $LaCoO_3$ and $Ru/LaCoO_3$-derived catalysts under reaction. For the used catalysts, the XRD and XPS analyses revealed a greater cobalt exposure and cobalt–lanthanum contact in catalyst with Ru (Table 4). This may be related with the lower size of the perovskite crystallites detected in the $Ru/LaCoO_3$ sample or to a promoting effect of ruthenium, preventing the sintering of cobalt atoms from perovskite reduction [29].

The different catalytic behaviour of the $Ru/LaCoO_3$ system could be related to the existence of more tightly bound oxygen (structural bulk oxygen) released during activation at 1125 K, as shown by the TPD-MS analysis. This mobility of oxygen within the crystal lattice of the solid could be responsible, at least in part, for the catalytic activity by favouring the adsorption of reactants from the gas phase [39]. Taking into account that the reaction temperature is close to this available oxygen at high temperature, it would be possible to propose the participation of this structural bulk oxygen in the reaction with the Ru-containing catalyst. Thus, different surface properties of perovskites, such as the presence of impurities of the single oxides, segregated Co_3O_4 [40,41], or the existence of more than one surface oxygen species, could modify both the adsorption and the catalytic properties [42].

Catalyst deactivation due to the formation of carbon is another factor to be considered in order to describe the evolution of the catalysts under reaction. As seen in Table 4, lower quantities of carbonaceous deposits were observed for the Ru-catalyst with respect to bare $LaCoO_3$. It is known [12,43,44] that higher carbonaceous deposits appear on metal particles of larger size and that the nature of the support plays a major role in assisting coke removal. Consistent with this, the higher cobalt dispersion observed for the $Ru/LaCoO_3$ used sample (Table 4) could contribute to the lower carbon concentration in this catalyst. Additionally, the lower degree of carbon deposition could also be related to the presence of La in the formulation. In the literature, the positive effects of lanthanum as a support of noble metals applied to the SR of hydrocarbons are explained in terms of the ability of lanthanum to adsorb CO_2, forming lanthanum oxycarbonates, which participate in coke gasification [45–47]. Some differences in the carbonate surface concentration in the used catalysts were found with XPS (Table 4). Thus, the concentration of these surface oxygen species is lower in the less stable $LaCoO_3$-derived catalyst than in the $Ru/LaCoO_3$-derived one.

The greater proportion of surface carbonates in the Ru-containing sample is in accordance with the smaller La_2O_3 particle size found by XRD for this sample (Table 4), since this would increase La_2O_3 dispersion, and consequently the formation of $La_2O_2CO_3$. Therefore, it may be inferred that lanthanum participates to some extent, probably through an enhanced adsorption of CO_2 increasing the lanthanum carbonate concentration, in the improvement in catalytic stability observed for the $Ru/LaCoO_3$-derived catalyst.

Although Ru has been found as more active for the steam reforming reaction of liquid hydrocarbons (C_7H_{14}) to produce hydrogen [48], the results obtained in this work with Ru/La_2O_3 and Ru/Co_3O_4 for the oxidative reforming of commercial diesel point to a lesser active and stable catalysts when compared to $Ru/LaCoO_3$-derived catalyst. From the results presented here both effects – higher cobalt dispersion and a lower carbon deposition related to the greater surface lanthana exposition – contribute to the observed enhancement in the reforming capacity and stability of $LaCoO_3$-derived catalysts with the incorporation of Ru. However, it should not be overlooked the involvement of ruthenium as active phase in the reaction and a deeper study using different ruthenium precursors as well as partial substitutions of cobalt by ruthenium in lanthanum perovskites is planned with the aim to elucidate the role of ruthenium both as active phase and restructuring the morphology of perovskite crystals.

5. Conclusions

Ruthenium added to $LaCoO_3$ increases the activity and stability of the $LaCoO_3$-derived catalyst for hydrogen production by oxidative reforming of diesel. Reorganization of the $LaCoO_3$ during Ru deposition leads to a lower particle size of the $LaCoO_3$ crystallites and greater surface cobalt segregation. The modifications in $LaCoO_3$ due to the addition of Ru directly affect the structure and morphology of the Co particles after the pretreatment in an inert atmosphere prior to the reaction. In the Ru-containing sample, the partial decomposition of perovskite in cobalt and lanthanum oxides during activation is inhibited, resulting in a well-defined perovskite structure at the beginning of the reaction. The active phases at the beginning of the reaction evolve differently with time on-stream. Although, it should not be overlooked the involvement of ruthenium as active phase in the reaction, it was found a higher proportion of perovskite phase in $Ru/LaCoO_3$, that produces during reaction a greater metallic cobalt and lanthanum oxide surface proportion, thus favouring the increase in catalyst stability. The greater cobalt exposure and cobalt–lanthanum contact achieved in the $Ru/LaCoO_3$ system, related to the lower size of the perovskite crystallites detected in the $Ru/LaCoO_3$ sample, and/or a promoting effect of ruthenium by preventing the sintering of cobalt atoms, contribute to the observed better catalytic stability in the catalyst with Ru. The better catalytic behaviour of the Ru-containing sample could be also related to the participation of bulk oxygen during the reaction, favouring adsorption of the reactants. Additionally, some participation of lanthanum in the better stability of the Ru-containing catalyst through an enhanced adsorption of CO_2 by increasing the formation of lanthanum carbonates, which participate in coke gasification, is inferred.

Acknowledgements

This work was carried out with the framework of the Project ''Development of a Diesel fuel processor'' carried out at the Instituto Nacional de Técnica Aerospacial (INTA), Centro de Investigación y Desarrollo en Automoción (CIDAUT) and the Instituto de Catálisis y Petroleoquímica (CSIC). RMN and MCAG acknowledge financial support from the MCYT in the Ramon y Cajal research program. We thank J.M. Frontela (Centro de Investigación de CEPSA) for kindly supplying the diesel used in the activity tests.

References

[1] J.C. Amphlett, R.F. Mann, B.A. Pepley, P.R. Roberge, A. Rodrigues, J.P. Salvador, J. Power Sources 71 (1998) 179.
[2] A.F. Ghenciu, Curr. Opin. Solid State Mater. Sci. 6 (2002) 389.
[3] M. Krumpelt, T.R. Krause, J.D. Carter, J.P. Kopasz, S. Ahmed, Catal. Today 77 (2002) 3.
[4] M. Ferrandon, T. Krause, Appl. Catal. A: Gen. 311 (2006) 135.
[5] E. Newson, T.B. Truong, Int. J. Hydr. Energy 28 (2003) 1379.
[6] M. Krumpelt, T. Krause, J.D. Carter, J. Mawdsley, J.-M. Bae, S. Ahmed, C. Rossignol, Catalytic Autothermal Reforming, 2001 DOE Annual Progress Report, Fuel Cells for Transportation.
[7] S. Muller, K. Striebel, O. Haas, Electrochim. Acta 39 (11/12) (1994) 1661.
[8] M.R. Goldwasser, M.E. Rivas, E. Pietri, M.J. Pérez-Zurita, M.L. Cubeiro, L. Gingembre, L. Leclercq, G. Leclercq, Appl. Catal. A: Gen. 255 (2003) 45.
[9] E. Pietri, A. Barrios, O. Gonzalez, M.R. Goldwasser, M.J. Pérez-Zurita, M.L. Cubeiro, J. Goldwasser, L. Leclercq, G. Leclercq, Stud. Surf. Sci. Catal. 136 (2001) 381.
[10] K. Tomishige, S. Kanazawa, K. Suzuki, M. Asadullah, M. Sato, K. Ikushima, K. Kunimori, Appl. Catal. A: Gen. 233 (2002) 35.
[11] M.A. Peña, J.L.G. Fierro, Chem. Rev. 101 (2001) 1981.
[12] M.R. Goldwasser, M.E. Rivas, E. Pietri, M.J. Pérez-Zurita, M.L. Cubeiro, A. Grivobal-Constant, G. Leclercq, J. Mol. Catal. A 228 (2005) 325.
[13] L.F. Brown, Int. J. Hydr. Energy 26 (2001) 381.
[14] S. Ahmed, M. Krumpelt, Int. J. Hydr. Energy 26 (2001) 381.
[15] A. Qi, S. Wang, G. Fu, C. Ni, D. Wu, Appl. Catal. A: Gen. 281 (2005) 233.
[16] J. Mawdsley, M. Ferrandon, C. Rossignol, J. Ralph, L. Miller, J. Kopasz, T. Krause, Hydrogen Fuel Cells and Infrastructure Technologies, Merit Review, Berkeley, 2003.
[17] A. Slagtern, U. Olsbye, Appl. Catal.: Gen. 110 (1994) 99.
[18] S. Cimino, G. Landi, L. Lisi, G. Russo, Catal. Today 105 (2005) 718.
[19] D. Liu, M. Krumpelt, Int. J. Appl. Ceram. Technol. 2 (4) (2005) 301.
[20] F. Simonot, G. Garin, G. Maire, Appl. Catal. B: Environ. 11 (1997) 167.
[21] C.D. Wagner, L.E. Davis, M.V. Zeller, J.A. Taylor, R.H. Raymond, L.H. Gale, Surf. Interf. Anal. 3 (1981) 211.
[22] J.F. Moulder, W.F. Stickle, P.E. Sobol, K.D. Bomben, in: J. Chastain (Ed.), Handbook of X-ray Photoelectron Spectroscopy, Perkin-Elmer Corporation, Eden Prairie, MN, 1992.
[23] R.M.G. de la Cruz, H. Falcon, M.A. Peña, J.L.G. Fierro, Appl. Catal. B: Environ. 33 (2001) 45.
[24] E.A. Lombardo, K. Tanaka, I. Toyoshima, J. Catal. 80 (1983) 340.
[25] E.V. Frolova, M. Ivanoskaya, V. Sadykov, G. Alikina, A. Lukashevich, S. Neophytides, Prog. Solid State Chem. 33 (2005) 317.
[26] T. Nakamura, T. Petzov, L.J. Gauckler, Res. Bull. 14 (1979) 649.
[27] M. Crespin, W.K. Hall, J. Catal. 69 (1981) 359.
[28] V. Szabo, M. Bassir, A. van Neste, S. Kaliaguine, Appl. Catal. B 37 (2002) 175.
[29] L. Huang, M. Bassir, S. Kaliaguine, Appl. Surf. Sci. 243 (2005) 360.
[30] S.A. Hosseini, A. Taeb, F. Feyzi, F. Yaripour, Catal. Commun. 5 (2004) 137.
[31] E. Iglesia, S.L. Soled, R.A. Fiato, G.H. Via, J. Catal. 143 (1993) 345.
[32] J. Dullac, Bull. Soc. Fr. Mineral Crystallogr. 92 (1969) 487.
[33] A. Galtayries, G. Blanco, G.A. Cifredo, D. Finol, J.M. Gatica, J.M. Pintado, H. Vidal, R. Sporken, S. Bernal, Surf. Interf. Anal. 27 (1999) 941.
[34] N. Yamazoe, Y. Teraoka, T. Seiyama, Chem. Lett. (1981) 1767.
[35] J. Kirchnerova, M. Alifanti, B. Delmon, Appl. Catal. A: Gen. 231 (2002) 65.
[36] N. Russo, D. Fino, G. Saracco, V. Specchia, J. Catal. 229 (2005) 459.

[37] L.G. Tejuca, J.L.G. Fierro, J.M.D. Tascón, Adv. Catal. 36 (1989) 237.
[38] S. Kaliaguine, A. Van Neste, V. Szabo, J.E. Gallot, M. Bassir, R. Muzychuk, Appl. Catal. A: Gen. 209 (2001) 345.
[39] D. Ferri, L. Forni, Appl. Catal. B: Environ. 16 (1998) 119.
[40] L. Forni, C. Oliva, F.P. Vatti, M.A. Kandala, A.M. Ezerets, V.V. Vishniakov, Appl. Catal. B: Environ. 7 (1996) 269.
[41] L. Simonot, F. Garin, G. Maire, Appl. Catal. B: Environ. 11 (1997) 181.
[42] J.L.G. Fierro, Catal. Today 8 (1990) 153.
[43] J.R. Rostrup-Nielsen, Catal. Today 63 (2000) 159.
[44] R. Lago, G. Bini, M.A. Peña, J.L.G. Fierro, J. Catal. 167 (1997) 198.
[45] Z.L. Zhang, X.E. Verykios, Appl. Catal. A: Gen. 138 (1996) 109.
[46] A. Slagtern, Y. Schuurman, C. Leclercq, X. Verykios, C. Mirodatos, J. Catal. 172 (1997) 118.
[47] A.N. Fatsikostas, D.I. Kondarides, X.E. Verykios, Catal. Today 75 (2002) 145.
[48] L. Wang, K. Murata, M. Inaba, Appl. Catal. A: Gen. 257 (2004) 43.